



Published in final edited form as:

J Med Chem. 2008 July 10; 51(13): 3731–3741. doi:10.1021/jm701239a.

Potent Non-Nucleoside Inhibitors of the Measles Virus RNA-Dependent RNA Polymerase Complex

Aiming Sun^{†,*}, Jeong-Joong Yoon[§], Yan Yin, Andrew Prussia[†], Yutao Yang[†], Jaeki Min[†], Richard K. Plemper[§], and James P. Snyder^{†,*}

[†]*Department of Chemistry, 1515 Dickey Drive, Emory University, Atlanta, GA 30322*

[§]*Department of Pediatrics, Division of Pediatric Infectious Diseases, Emory Children's Center, 2015 Uppergate Drive, Emory University School of Medicine, Atlanta, GA 30322*

Abstract

Measles virus (MV) is one of the most infectious pathogens known. In spite of the existence of a vaccine, approximately 350,000 deaths/year result from MV or associated complications. Anti-measles compounds could conceivably diminish these statistics and provide a therapy that complements vaccine treatment. We recently described a high-throughput screening hit compound **1** (16677) against MV-infected cells with the capacity to eliminate viral reproduction at 250 nM by inhibiting the action of the virus's RNA-dependent RNA polymerase complex (RdRp). The

¹Abbreviations

MV	measles virus
CPE	cytopathic effect
MTT	[3-(4,5-dimethylthiazol-2-yl)-2,5-diphenyltetrazolium bromide]
MV-Edm	measles virus Edmonston strain
RdRp	RNA-dependent RNA polymerase
CC ₅₀	compound concentration that returns 50% cytotoxicity
EC ₅₀	compound concentration that returns 50% inhibition
SI	selectivity index, defined as CC ₅₀ /EC ₅₀
SAR	structural activity relationship
QSAR	quantitative structural activity relationship
MFTA	molecular field topology analysis

*Corresponding authors: Phone: 404-727-6689 ; Fax: 404-727-6689; e-mail: asun2@emory.edu Phone: 404-727-2415; Fax: 404-727-6586; e-mail: jsnyder@emory.edu

compound, 1-methyl-3-(trifluoromethyl)-*N*-[4-sulfonylphenyl]-1H-pyrazole-5-carboxamide, carries a critical CF₃ moiety on the 1,2-pyrazole ring. Elaborating on the preliminary structure-activity (SAR) study, the present work presents the synthesis and SAR of a much broader range of low nanomolar non-peptidic MV inhibitors and speculates on the role of the CF₃ functionality.¹

Keywords

measles virus; high-throughput screening (HTS); pyrazoles

Introduction

Paramyxoviruses are negative stranded RNA viruses, most of which are highly contagious airborne pathogens that spread via the respiratory route. Members of this viral family include major human and animal pathogens such as measles virus (MV), human parainfluenza viruses (HPIV), mumps virus, respiratory syncytial virus and Newcastle disease virus.¹ Despite the existence of an effective live-attenuated vaccine,² MV remains a serious threat to human health globally, accounting for approximately 0.35 million deaths annually.³ While most of these cases occur in developing countries with limited access to vaccination, measles outbreaks still occur in some developed countries that have failed to maintain high vaccine coverage rates. According to recent estimates, 20 million cases of measles occur annually worldwide. Current outbreaks in the developed world have affected Japan in the Western Pacific Region, Nova Scotia, New Brunswick, Prince Edward Island, and Ontario, Canada, and several parts of Western Europe.^{4,5a-c}

This is partially due to declining herd-immunity as a result of reduced vaccination coverage resulting from parental concerns about vaccination safety.⁶ Vaccination coverage below protective levels in areas of the developing world and continued viral activity in the developed world make desirable the development of novel therapeutics that can be used for the rapid control of local outbreaks and improved case management to limit severe outcomes of infection.

To date, Ribavirin, (**1a**) is the only drug available for the treatment of some paramyxovirus infections^{7,8} It has been used experimentally for the treatment of measles but with limited efficacy.⁹ More recently, benzimidazo-thiazole derivatives (**1b**) have been reported to be more potent and less cytotoxic compared with Ribavirin against the Leningrad 16 strain, when assessed in Vero (African green monkey kidney carcinoma) cells. The most active compound in this series demonstrated a selectivity ratio (CC₅₀/EC₅₀) of 245.5 compared with 14.4 for Ribavirin.¹⁰

In previous work we reported the structure-based development of a MV entry inhibitor, *N*-(5-amino-2-hydroxy-phenyl)-2-phenyl-acetamide (AS-4, Figure 1), with an EC₅₀ of 260 nM against the MV-Edmonston (MV-Edm) strain.^{11, 12} Since this compound proved to be unstable, we developed AS-48 with an EC₅₀ of 0.6-3.0 μM (Figure 1) as a shelf-stable alternative.^{11(b)} Further attempts to increase the activity within this series of compounds proved to be problematic. As a consequence, we broadened our search by turning to cell-based high throughput screening (HTS) to capture small molecules capable of netting both entry inhibitors as well as compounds operating against other proteins critical for viral infection and reproduction. The exercise identified 1-methyl-3-(trifluoromethyl)-*N*-[4-(pyrrolidinylsulfonyl)phenyl]-1H-pyrazole-5-carboxamide **1** (16677) (Figure 1) (EC₅₀ = 250 nM,) as a well-behaved, target-specific inhibitor of MV replication.¹³ Bypassing the fusion protein, **1** represents a first-in-class non-nucleoside inhibitor of the MV RNA-dependent RNA polymerase (RdRp) complex. Following re-synthesis of the hit compound **1**, by coupling 1-

methyl-3-trifluoro-pyrazole-5-acetyl chloride with 4-amino-prolidinyl sulfonamide **7a** in the presence of pyridine,¹⁴ previous preliminary structural modifications focused on the right side of the molecule as depicted in Figure 2a.¹⁵ In the present work, we describe optimization of antiviral activity for compound **1** scaffold by manipulation of the pyrazole (A) and pyrrolidine (D) rings.

Preparation of analogs around the HTS hit compound **1**

Modification of the pyrazole ring

The first stage of hit optimization introduced a variety of aromatic rings as 1-methyl-3-trifluoromethyl pyrazole replacements. Compounds **2a-o** (Figure 2b, **Table S1**) can be readily prepared by coupling the corresponding acetyl chlorides with 4-amino-prolidinyl sulfonamide **7a** in the presence of pyridine.¹⁵ Preliminary efforts were also devoted to modifying the 1-methyl-3-trifluoromethyl-pyrazole ring. For example, the corresponding 4-bromo-1-methyl-3-(trifluoromethyl)-*1H*-pyrazole-5-carboxylic acid was prepared by the protocol reported by Schlosser and treated with oxalyl chloride to obtain acetyl chloride **3**. The latter was further coupled with sulfonamide **7a** to give the 4-bromo-substituted analog **4**. (Scheme 1)

In the present work, 3-trifluoromethyl pyrazole was treated with NaH in DMF, followed by regioselective benzylation and alkylation to obtain 1-benzyl or alkyl-3-trifluoromethylpyrazole. The compound was then subjected to a routine deprotonation-carboxylation sequence before coupling with aniline **7c** to obtain the desired compounds **9**. (Scheme 2)

2-Methoxycarbonylphenyl and 2-carboxyphenyl analogs were also prepared as outlined in Scheme 3. The furan precursor **10** was obtained as previously described¹⁶ and converted to ester **11** via the acid chloride/methylation method. Oxidation of the furyl functionality afforded the desired carboxylic acid **12**. The latter as its acid chloride was coupled to aniline **7a** to afford compound **13**. Saponification of ester **13** provided the corresponding acid **14**.

Syntheses of **23**, **24**, **28** and **29** proved to be straightforward by following standard procedures for sulfonamide analogs as illustrated in **Schemes 4** and **5**. For example, combination of 4-nitro-benzenesulfonyl chloride with pyrrolidine afforded 4-nitro-pyrrolidinyl sulfonamide **6**. The latter was reduced either with SnCl₂ in EtOAc or by hydrogenation over Pd/C (5%) to obtain 4-amino-prolidinyl sulfonamide **7** in almost quantitative yield. Other secondary amides behave similarly. Coupling of **7** with 1-methyl-3-(trifluoromethyl)-*1H*-pyrazole-5-carbonyl chloride obtained compound **23**. De-protection of Boc-groups with a mixture of TFA and CH₂Cl₂ (3:1) at room temperature for about 4h delivers free amines **24e** and **24f**. Compounds **29e** and **29f** were obtained by hydrolysis of the corresponding esters **28** in 1N HCl. Analogs **15a-r**¹⁵ (See Table 1) were prepared by using the same procedure as described in Scheme 4.

Qualitative SAR for compound **1** analogs

Disappointedly, all attempts to replace the pyrazole ring with 5- or 6-membered aromatic rings¹⁵ or to alter substituents on the pyrazole ring (e.g. **4**, **13** and **14**) led either to a decrease or to a complete loss of activity. A striking example is the inactivity of the series of *N*-alkyl analogs of **1** (EC₅₀ 30-150 nM¹⁵). Replacement of the *N*-methyl with *N*-isopropyl or *N*-benzyl (**9b** and **c**, respectively) leads to disappearance of potency in the virus titer reduction assay. While the *N*-ethyl pyrazole **9a** demonstrates good activity in (EC₅₀ = 55 nM), the compound is highly toxic. In a previous limited exploration of the SAR of **1**, we learned that installing a piperidine ring instead of the pyrrolidine ring on the left side of the molecule (Figure 2a, **D ring**) provided a 100-fold boost in activity while simultaneously delivering very low toxicity.¹⁵ To exploit this potency advantage, a variety of alicyclic heterocyclic rings (**15a-l**) or dialkyl

amines (**15m-r**) were employed as pyrrolidine replacements while retaining the remainder of compound **1** structure (see Table 1).

Piperidine analogs **15a-e** and **15k** exhibit significant potency improvements by comparison with the original hit. All yield EC₅₀s in the low nM range. The 2-ethyl substitution on the piperidine ring in **15e** elicits 2-6 fold less activity than methyl substitution (**15b-15d**). The seven membered ring variant **15f** is 10-fold more potent than the azacyclooctane analog **15g** and about 3-fold more active than the piperidine **15a**. However, C2-substitution of the pyrrolidine ring with either an ester or a carboxylic acid (**15h** and **15i**, respectively) greatly decreases activity by about 100-fold as does introduction of an indole ring (**15j**). Interestingly, while the open-chain diethyl amine compound **15n** is highly active, the alkyl-enhanced di-isopropyl, dipropyl and diallyl variants **15o**, and **15p** and **15r** lose 10-20 fold potency by comparison. Similarly, **15m** and **15q**, the dimethyl and di-isobutyl analogs, respectively, exhibit drops in activity.

Additional structural modifications of compound **1** included synthesis of **16-20**, compounds that examine structural environments around a 6-membered ring. (Figure 3) Analog **16** moves the nitrogen out of the piperidine ring of **15a** and introduces a secondary amine as an H-bond donor, while **17** incorporates a sulfonate moiety instead of a sulfonamide group. Compound **18** incorporates a methyl group on the amide and eliminates possible hydrogen bonding of NH with a nearby amino acid residue. All three compounds **16**, **17** and **18** occasion a complete loss of activity. Compounds **19** and **20** switch the sulfonamide *para*-amide linker in sector C to the *meta*- and *ortho*-positions, respectively. Both compounds **19** and **20** similarly show no detectable activity below 75 μM. (Table 1)

Discovery of four highly active piperidine analogs in the D-sector of **1** (**15a-d**, see Table 1 for biological data) encouraged us to further examine this center in an effort to retain nM potency while improving solubility within the series. Thus, morpholine derivative **23a**, piperazines **23b-d** and **24e** and piperidine rings decorated with hydrophilic groups **24f**, **28a-d** and **29e-f** were prepared. Unfortunately, with the exception of **28c** bearing a CH₂OH group alpha to nitrogen (EC₅₀ 850 nM), none of the compounds are significantly active. Clearly, the incorporation of a hydrophilic group in this sector is detrimental to MV blockade (Table 1). This may reflect impaired passive diffusion through the plasma membrane, since inhibitors of the RdRp complex activity need access to the cytosol of the infected cells.

Molecular Field Topology Analysis (MFTA) QSAR

The SAR discussion in the previous section is based on qualitative observations. In an effort to put this on a more quantitative footing, the MFTA method developed by Palyulin et al.^{17, 18} was applied to the MV RdRp complex inhibitor series to generate a quantitative structure-activity relationship (QSAR). MFTA performs a topological analysis for a compound series, generates a molecular supergraph with descriptor values for each compound mapped at each atom vertex, and finishes with PLS-based correlation statistics to generate predictive QSAR models. In the present case, the log(1/EC₅₀) values for CPE inhibition without standard deviations were used as the numerical biological endpoints. To incorporate the virus titer data into the correlation, the titer values of compounds with CPE inhibitory activities less than 2.3 μM were scaled to an equivalent CPE EC₅₀ by a conversion factor of 10 μM EC₅₀ per 1 μM virus titer. The latter was based on the EC₅₀s and virus titers for **15o** and **28d**. Where compounds exhibit activities greater than 75 μM, a value of 150 μM was assigned. Compounds with a cytotoxicity greater than 300 μM or a therapeutic index greater than 4 were selected for MFTA. To simplify the analysis within a congeneric series, only compounds with a scaffold similar to the pyrazole ring A, amide linker B, and sulfonamide linker C were included. Thus, the training set consisted of 26 compounds: **1**, **2j**, **2o**, **9a**, **13**, **14**, **15a**, **15c-15i**, **15k**, **15m**, **15o**, **15p**, **15r**, **23a**, **23d**, **28c**, and **28d**. Three compounds from a previous publication¹⁵ were also included

because they are instructive members of this congeneric series (cf. **S5**, **S7** and **S8**, **Figure S1**). On the other hand, **9b**, **23c**, **24f**, **29e**, and **29f** were inactive and consistent outliers. Thus, these compounds were excluded from the training set. For the test set, 7 compounds were used **2n**, **2k**, **15b**, **15n**, **24e**, **28a**, and **S6** (**Figure S1**).¹⁵

A variety of single local descriptors and sets of local descriptors were applied to the training set, generating a series of different models with varying predictive Q^2 values based on MFTA's leave-25%-cross-validation. The best results were obtained with descriptors for Gasteiger-Marsili atomic charge (Q), the effective environment van der Waal radius (R_e), and group lipophilicity based on the sum of the Ghose-Crippen atomic contributions for an atom and attached hydrogens (L_g). This QSAR model generated a correlation (Figure 6) with the following statistics: $N = 26$, number of PLS factors $N_F = 2$, $R = 0.88$, $R^2 = 0.77$, $RMSE = 0.49$, and $Q^2 = 0.66$. Adding additional descriptors did not substantially improve the correlation. To verify that MFTA has not simply fortuitously found a non-predictive model, a Y-randomization test³⁸ was performed on the training set data in ten separate trials. In each trial the activity data was randomly re-ordered, and a QSAR model generated. Each random data set delivered the same mean, variance, and molecular supergraph, but no real correlation of activity to structure. The resulting QSAR models generally had a good correlation ($R_{avg} = 0.83$, $R_{max} = 0.92$), but poor predictive ability ($Q^2_{avg} = 0.21$, $Q^2_{max} = 0.42$). This lends confidence that the experimental model with $Q^2 = 0.66$ is not an artifact of the method.

Predictions for the seven compound test set with the present model were made by first using MFTA to map the test set compounds with assigned descriptor values to the previously generated molecular supergraph, followed by prediction with the PLS model based on the training set (Figure 5). Test set activities are predicted reasonably well with $R = 0.67$ and $R^2 = 0.45$. For three of the compounds, the errors are somewhat substantial (about 30-40% of the training set activity span in log units), but for the other 4 compounds the error is less than 20%. The mean absolute error for the complete test set is 0.74 log units, and the RMS error of prediction is 0.86 log units.

MFTA was used to visualize the descriptors' contributions to the correlation by means of a color-coded molecular supergraph (Figure 6). Positions colored brown and red suggest that an increase in descriptor property in that part of the molecule would increase activity, red positions having more effect than brown. Conversely, light blue and blue positions suggest that an increase in descriptor property would decrease activity, blue positions having more effect than light blue. At uncolored positions, either the descriptor property is not correlated to activity, or there is insufficient diversity in the training set for MFTA to develop correlation to activity. The reader should note that the attempt to display the range of substituents in 2D in sector D in Figure 6 leaves the impression of disorder around the sulfonyl amine group. This is inaccurate and misleading, since the correlation of descriptor property to activity is limited by the property range of the substituents in the training set. The graph accurately reflects how subtle changes in the atoms' properties affect activity within the bounds of diversity in the training set.

Interpreting the descriptor impact graphs supports qualitative trends in the structure-activity data. Substituted rings and alkyl chains attached to the sulfonamide have a positive impact on activity if they increase the lipophilicity and decrease the charge on this part of the molecule. However, the QSAR model is able to parse some additional complexity in the structure-activity data by noting that increasing charge in the 3- and 4-positions of the pyrrolidine ring, as well as the *para*-position of the 6-membered ring, has a favorable effect on activity. In general, substituents connected to the pyrazole ring have a favorable impact on activity, if they contribute an increase in size and lipophilicity. Increasing charge at the pyrazole ring can either positively or negatively effect activity, depending on the substituent position.

Discussion

Mechanistic and functional characterization of the high-throughput screening hit **1** has demonstrated that the compound represents a first-in-class non-nucleoside inhibitor of MV RdRp complex activity.¹³ We have developed an SAR by structural manipulation of **1** within the four sectors highlighted in Figure 2a. Previously published work¹⁵ has been focused mainly on the phenyl sulfonamide unit, the amide linker and the pyrazole ring in sector A. A variety of modifications within sector A-C either essentially abolish anti-MV activity or result in high cytotoxicity. However, a highly potent analog has been identified by replacing the pyrrolidine ring in compound **1** with a piperidine. Subsequent SAR development of the current series was centered on modification of the heterocyclic rings in sectors A and C. Disappointedly, all attempts to replace the N-methyl group on the pyrazole ring (**9a-c**, **13** and **14**) or to add other functionality on the same ring leads to complete loss of activity or high toxicity (**9a**). Furthermore, replacement of the pyrazole ring CF₃ group with Me or *t*-Bu also causes significant loss of activity, a factor explained below by the beneficial electrostatic properties of the CF₃ group.

Intriguingly, maintaining the structure of the hit molecule **1** in sectors A-C, while modifying the pyrrolidine ring in D, delivers highly active and non-cytotoxic compounds. (Table 1, **15a-g**, **15k**) The seven-membered ring analog **15f** was the most potent series member with an EC₅₀ around 5 nM and no detectable cytotoxicity at concentrations below 300 μM as determined by two independent assays (reflected by an approximate selectivity index (CC₅₀/EC₅₀) of 85,000). Further increases in the ring size, however, resulted in a reduction of antiviral activity by about 10-fold (Table 1, **15g**). The open chain diethyl amine analog **15n** also exhibited excellent antiviral activity. However, other amine substitutions (**15o** and **15q**) caused a complete loss of activity.

Further optimization of the lead compound sought to increase solubility and improve cellular bioavailability. Such structural changes may, of course, reduce membrane-permeability and consequently compromise antiviral activity. In attempts to resolve the conflicting structural requirements, compounds with a piperazine ring (**24e**) and polar groups on the piperidine (e.g. **24d,f** and **28a-f**, Figure 2a, sector D) were prepared. Indeed, assessment of biological activity returned a correlation between increasing hydrophilicity and decreasing inhibitory potency. Within this series, all compounds were completely inactive with the exception of piperidines **28c** and **28d**, which harbor 2-CH₂OH and 4-OH groups, respectively; both returning only moderate activity.

Interactions between ligand CF₃ groups associated proteins

Compound **1**, the most potent high throughput screening (HTS) inhibitor against MV¹³ identified from a 34,000 compound pool,¹⁹ carries a trifluoromethyl group on the pyrazole ring. Substitution of the CF₃ with a methyl or a *t*-butyl group completely abrogates the inhibitory activity of the compound.¹⁵ In order to gain insight into the possible role of the pyrazole CF₃ as an enhancer of MV inhibition and to investigate more generally the structural influence of CF₃ groups in protein-bound ligands, we searched the Protein Data Bank (PDB) for such protein-ligand complexes using Relibase+ and ReliView. A total of 132 CF₃-complemented ligands was returned from the search. Less than a dozen trifluoromethyl groups are located in hydrophobic environments, while 15 are directed into the aqueous layer surrounding the proteins. Carbon-fluorine bonds in 117 complexes were judged to participate in at least one CF---HX (X = O, N or S, r(F---H) 1.8-2.0 Å) interaction in which F---X distances range from 2.7-3.6 Å. It has been argued that fluorine rarely engages in hydrogen bonds in small molecule X-ray crystal structures.²⁰ However, in protein pockets where ligands are immobilized by a variety of forces, they appear to be more common. F---X distances beyond 3.0 Å can be regarded as dipole-dipole interactions that most likely provide small stabilizing

contributions (≤ 1 kcal/mol) for the observed binding poses. An example is presented in Figure 7 showing the heterocyclic terminus of the rhinovirus blocker pleconaril encased in a hydrophobic pocket (PDB code 1NCR²¹). One of the CF₃ fluorine atoms experiences a short contact with the backbone NH of Tyr144.

A subset of 28 cases involve cationic Arg, Lys and His residues that direct N-H bonds toward fluorine. One interesting CF₃-protein association (1P2S22) locates the fluorinated moiety of 2,2,2-trifluoroethanol (CF₃CH₂OH) between Arg and Lys side chains in H-Ras 166 as shown in Figure 8.

The topographical representation shows that Arg97 forms a bidentate contact with two fluorine atoms, while Lys101 associates with one fluorine in the same pair; all of which involve F...H distances of 2.6-2.7 Å. The latter are 0.3-0.4 Å smaller than the sum of the van der Waals radii (N 1.55, F 1.47 Å).²³ These charge-dipole interactions are well known to operate as controlling forces in the conformational preferences of fluorinated piperidines. In particular, the fluorine in protonated 3-fluoropiperidines universally adopts an axial orientation contrary to intuition based on cyclohexane conformational analysis.^{24, 25}

Figure 9 depicts a trifluoromethyl ketone inhibitor of human leukocyte elastase (1EAS26). The compound enjoys a weak interaction with the SH of Cys42 and a stronger association with His57. Intriguingly, four protein ligands incorporate CF₃-substituted pyrazole rings very similar to that found in compound **1**. Three of these (1X7A,²⁷ 1CX2²⁸ and 6COX²⁹) juxtapose the CF₃ fluorines and a single Arg residue located among hydrophobic residues. This observation has been exploited to explain the activity of a series of anti-inflammatory COX inhibitors.³⁰ Porcine Factor IXa complexed to 1-{3-[amino(imino)methyl]phenyl}-N-[4-(1H-benzimidazol-1-yl)-2-fluorophenyl]-3-(trifluoromethyl)-1H-pyrazole-5-carboxamide (1X7A) is illustrative (Figure 10). The fourth CF₃-substituted pyrazole ligand, a nanomolar inhibitor of carbonic anhydrase (1OQ530) positions the trifluoromethyl group in a hydrophobic cavity on the surface of the protein partially exposed to the aqueous layer surrounding the protein.

If the binding site for pyrazole in the MV RNA-dependent RNA polymerase were hydrophobic or solvent exposed, then substitution of CF₃ in compound **1** with CH₃ (Figure 2b, **2n**) is unlikely to cause complete loss of activity as observed. Consequently, we conclude that the pyrazole-CF₃ in the highly active MV blockers examined in this work (Table 1, **15a-g**, **15k&15n**) is likely docked in a pocket that house either a cationic Arg, His or Lys. This prediction is being actively pursued to identify MV blockers which maintain potency but carry improved solubility and bioavailability properties.

Conclusions

High throughput screening followed by chemical synthesis has provided the first highly potent small molecule blockers of the measles virus accompanied by low cell toxicity. Synthetic modification of the **1** lead reveals that both potency gains and structural diversity resides primarily in sector D (Figure 2a). This behavior is captured by a three-descriptor QSAR model developed using molecular field topology analysis (MFTA) and implies the sector D sulfonyl amines reside in a rather tight hydrophobic cavity. Behavior at the other end of the molecule (sector A), suggests that the pyrazole-CF₃ most likely sits in a pocket housing cationic Arg, His or Lys. These speculations are being actively pursued in an effort to identify MV blockers which maintain potency but carry improved solubility and bioavailability properties suitable for evaluating various MV strains and closely related viruses in animal models

Supplementary Material

Refer to Web version on PubMed Central for supplementary material.

Acknowledgements

This work was supported by a research grant from the American Lung Association, and Public Health Service grants AI056179 and AI071002 from NIH/NIAID (to RKP) and by the National Institutes of Health 1 U54 HG003918 (to JPS). We are grateful to Ernest Murray for synthetic assistance

References

- (1). Lamb, RA.; Kolakosky, D. Paramyxoviruses: The viruses and their replication. In: Fields, BN.; Knipe, DM.; Howley, PM., editors. *Fundamental Virology*. Lippencott-Raven; Philadelphia, PA: 1996. p. 577-604.
- (2). Hilleman MR. Current overview of the pathogenesis and prophylaxis of measles with focus on practical implications. *Vaccine* 2001;20:651-665. [PubMed: 11738730]
- (3). CDC. Progress in Reducing Measles Mortality - Worldwide, 1999-2003. *MMWR* 2005;54:200-203. [PubMed: 15744229]
- (4). Gans HA, Arvin AM, Galinus J, Logan L, DeHovitz R, Maldonado Y. Deficiency of the humoral immune response to measles vaccine in infants immunized at age 6 months. *JAMA* 1998;280:527-532. [PubMed: 9707142]
- (5)(a). Polack FP, Lee SH, Permar S, Manyara E, Nousari HG, Jeng Y, Mustafa F, Valsamakis A, Adams RJ, Robinson HL, Griffin DE. Successful DNA immunization against measles: neutralizing antibody against either the hemagglutinin or fusion glycoprotein protects rhesus macaques without evidence of atypical measles. *Nat. Med* 2000;6:776-781. [PubMed: 10888926] (b) Wichmann O, Hellenbrand W, Sagebiel D, Santibanez S, Ahlemeyer G, Vogt G, Siedler A, van Treeck U. Large measles outbreak at a German public school, 2006. *Pediatr. Infect. Dis. J* 2007;26:782. [PubMed: 17721371] (c) Chironna M, Prato R, Sallustio A, Martinelli D, Germinario C, Lopalco P, Quarto M. Genetic characterization of measles virus strains isolated during an epidemic cluster in Puglia, Italy. *Viol J* 2007;21:90. [PubMed: 17888162]
- (6). Jansen VA, Stollenwerk N, Jensen HJ, Ramsay ME, Edmunds WJ, Rhodes CJ. Measles outbreaks in a population with declining vaccine uptake. *Science* 2003;301:804. [PubMed: 12907792]
- (7). Shigeta, Shiro; Shuichi, Mori; Masanori, Baba; Masahiko, Ito; Honzumi, Ken; Nakamura, Kiyoto; Oshitani, Hitoshi; Numazaki, Yoshio; Matsuda, Akira, et al. Antiviral activities of ribavirin, 5-ethynyl-1-beta -D-ribofuranosylimidazole-4-carboxamide, and 6'-(R)-6'-C-methylneplanocin A against several ortho- and paramyxoviruses. *Antivir. Chem. Chemother* 1992;36:435-9.
- (8). Gabrielsen, Bjarne; Phelan, Michael J.; Barthel-Rosa, Luis; Cathy; Huggins, John W.; Kefauver, Deborah F.; Monath, Thomas P.; Ussery, Michael A.; Chmurny, Gwendolyn N., et al. Synthesis and antiviral evaluation of N-carboxamide-substituted analogs of 1-beta-D-ribofuranosyl-1,2,4-triazole-3-carboxamide hydrochloride. *J. Med. Chem* 1992;35:3231-3238. [PubMed: 1507208] See
- (9). Barnard DL. Inhibitors of measles virus. *Antivir. Chem. Chemother* 2004;15:111-9. [PubMed: 15266893]
- (10). Pokrovskii AG, Il'icheva TN, Kotovskaya SK, Romanova SA, Charushin VN, Chupakhin ON. Fluorinated Derivatives of Benz[4,5]imidazo[1,2-b][1,3] thiazole—Inhibitors of Reproduction of Measles Virus. *Doklady Biochem. Biophys* 2004;398:285-287.
- (11)(a). Plemper RK, Erlandson KJ, Lakdawala AS, Sun A, Prussia AJ, Boonsombat J, Aki-Sener E, Yalcin I, Yildiz I, Temiz-Arpaci O, Tekiner B, Liotta DC, Snyder JP, Compans RW. *Proc. Natl. Acad. Sci. USA* 2004;101:5628-5633. [PubMed: 15056763] (b) Sun A, Prussia A, Zhan W, Murray EE, Doyle J, Cheng LT, Yoon JJ, Radchenko EV, Palyulin VA, Compans RW, Liotta DC, Plemper RK, Snyder JP. *J Med. Chem* 2006;49:5080-5092. [PubMed: 16913698]
- (12). Plemper RK, Lakdawala AS, Gernert KM, Snyder JP, Compans RW. *Biochemistry* 2003;42:6645-6655. [PubMed: 12779319]

- (13). White LK, Yoon J-J, Lee JK, Sun A, Du Y, Fu H, Snyder JP, Plemper RK. Nonnucleoside Inhibitor of Measles Virus RNA-Dependent RNA Polymerase Complex Activity. *Antimic. Agents Chemother* 2007;51:2293–2303.
- (14). Schlosser M, Volle J, Leroux F, Schenk K. Switchable Reactivity: The site-Selective Functionalization of Trifluoromethyl Substituted Pyrazoles. *Eur. J. Org. Chem* 2002:2913–20.
- (15). Sun A, Chandrakumar N, Yoon J-J, Plemper RK, Snyder JP. Nonnucleoside inhibitors of the measles virus RNA-Dependent RNA polymerase activity: Synthesis and in vitro evaluation. *Bioorg. Med. Chem. Lett* 2007;17:5199–5203. [PubMed: 17643302]
- (16). Pruitt JR, Pinto DJP, Glemmo RA, Alexander RS, Rossi KA, Wells BL, Drummond S, Bostrom LL, Burdick D, Bruckner R, Chen H, Smallwood A, Wong PC, Wright MR, Bai S, Luetzgen JM, Knabb R, Lam PYS, Wexler RR. Discovery of 1-(2-Aminomethylphenyl)-3-trifluoromethyl-N-[3-fluoro-2'-(aminosulfonyl)[1,1'-biphenyl]-4-yl]-1H-pyrazole-5-carboxamide (DPC602), a Potent, Selective, and Orally Bioavailable Factor Xa Inhibitor. *J. Med. Chem* 2003;46:5298–5315. [PubMed: 14640539]
- (17). Palyulin VA, Radchenko EV, Zefirov NS. Molecular Field Topology Analysis Method in QSAR Studies of Organic Compounds. *J. Chem. Inf. Model* 2000;40:659–667.
- (18). Mel'nikov AA, Palyulin VA, Zefirov NS. Generation of molecular graphs for QSAR studies. *Dokl. Chem* 2005;402:81–85.
- (19). ChemDiv, Inc.. 6605 Nancy Ridge Drive. San Diego, CA: 92121; <http://www.chemdiv.com/en/products/screening/>
- (20). Dunitz JD, Taylor R. Organic Fluorine Hardly Ever Accepts Hydrogen Bonds. *Chem. Eur. J* 1997;3:89–98. Dunitz JD. Organic Fluorine: Odd Man Out. *Chem. Bio. Chem* 2004;5:614–621.
- (21). Zhang Y, Simpson AA, Ledford RM, Bator CM, Chakravarty S, Skochko GA, Demenczuk TM, Watanyar A, Pevear DC, Rossmann MG. Structural and virological studies of the stages of virus replication that are affected by antirhinovirus compounds. *J. Virol* 2004;78:11061–11069. [PubMed: 15452226]
- (22). Buhrman GK, de Serrano V, Mattos C. Organic Solvents Order the Dynamic Switch II in Ras Crystals. *Structure* 2003;11:747–751. [PubMed: 12842038]
- (23). Bondi A. van der Waals Volumes and Radii. *J. Phys. Chem* 1964;68:441–451.
- (24). Lankin DC, Chandrakumar NS, Rao SN, Spangler DP, Snyder JP. Protonated 3-Fluoropiperidines: An Unusual Fluoro Directing Effect and a Test for Quantitative Theories of Solvation. *J. Am. Chem. Soc* 1993;115:3356–3357. Snyder JP, Chandrakumar NS, Sato H, Lankin DC. The Unexpected Diaxial Orientation of *cis*-3,5-Difluoropiperidine in Water: A Potent CF- -NH Charge-Dipole Effect. *J. Am. Chem. Soc* 2000;122:544–545. Lankin DC, Grunewald GL, Romero FA, Oren IY, Snyder JP. The NH---FC Dipole Orientation Effect for Pendant Exocyclic CH₂F. *Org. Lett* 2002;4:3557–3560. [PubMed: 12375886] Sun A, Lankin DC, Hardcastle K, Snyder JP. 3-Fluoropiperidines and *N*-Methyl-3-fluoropiperidinium Salts: The Persistence of Axial Fluorine. *Chem. Eur. J* 2005;11:1579–1591.
- (25). Jensen HH, Lyngbye L, Jensen A, Bols M. Stereoelectronic Substituent Effects in Polyhydroxylated Piperidines and Hexahydropyridazines. *Chem. Eur. J* 2002;8:1218–1226. Jensen HH, Bols M. Stereoelectronic Substituent Effects. *Acc. Chem. Res* 2006;39:259–265. [PubMed: 16618093]
- (26). Bernstein PR, Andisik D, Bradley PK, Bryant CB, Ceccrelli C, Damewood JR Jr, Earley R, Edwards PD, Feeney S, Gomes BC, Kosmider BJ, Steelman GB, Thomas RM, Vacek EP, Veale CA, Williams JC, Wolanin DJ, Woolson SA. Nonpeptidic Inhibitors of Human Leukocyte Elastase. 3. Design, Synthesis, X-ray Crystallographic Analysis, and Structure-Activity Relationships for a Series of Orally Active 3-Amino-6-phenyl-2-pyridinyl Trifluoromethyl Ketones. *J. Med. Chem* 1994;37:3313–3326. [PubMed: 7932559]
- (27). Smallheer JM, Alexander RS, Wang J, Wang S, Nakajima S, Rossi KA, Smallwood A, Barbera F, Burdick D, Luetzgen JM, Knabb RM, Wexler RR, Jadhav PK. SAR and factor IXa crystal structure of a dual inhibitor of factors IXa and Xa. *Bioorg. Med. Chem. Lett* 2004;14:5263–5267. [PubMed: 15454208]
- (28). Kurumbail RG, Stevens AM, Gierse JK, McDonald JJ, Stegeman RA, Pak JY, Gildehaus D, Miyashiro JM, Penning TD, Seibert K, Isakson PC, Stallings WC. Structural basis for selective inhibition of cyclooxygenase-2 by anti-inflammatory agents. *Nature* 1996;384:644–648. [PubMed: 8967954]

- (29). Singh SK, Vobbalareddy S, Kalleda SR, Rajjak SA, Casturi SR, Datla SR, Mamidi RNVS, Mullangi R, Bhamidipati R, Ramanujam R, Akella V, Yeleswarapu KR. 2-Hydroxymethyl-4-[5-(4-methoxyphenyl)-3-trifluoromethyl-1*H*-1-pyrazolyl]-1-benzenesulfonamide (DRF-4367): an orally active COX-2 inhibitor identified through pharmacophoric modulation. *Org. Biomol. Chem* 2004;2:2442–2450. [PubMed: 15326524]
- (30). Weber A, Casini A, Heine A, Kuhn D, Supuran CT, Scozzafava A, Klebe G. Unexpected nanomolar inhibition of carbonic anhydrase by COX-2-selective celecoxib: new pharmacological opportunities due to related binding site recognition. *J. Med. Chem* 2004;47:550–557. [PubMed: 14736236]
- (31). Reaction of 4-nitro-benzene sulfonyl chloride with pyrrolidine in the presence of pyridine afforded 4-nitro-prolidinyl sulfonamide. Reduction with tin dichloride dihydrate in ethyl acetate provided 4-amino-prolidinyl sulfonamide **7a** in excellent yield (90%)
- (32). Berman HM, Westbrook J, Feng Z, Gilliland G, Bhat TN, Weissig H, Shindyalov IN, Bourne PE. The Protein Data Bank. *Nucleic Acids Res* 2000;28:235–242. [PubMed: 10592235]
- (33). Hendlich M, Bergner A, Gunther J, Klebe G. Relibase - Design and Development of a Database for Comprehensive Analysis of Protein-Ligand Interactions. *J. Mol. Biol* 2003;326:607–620. [PubMed: 12559926]
- (34). Günther J, Bergner A, Hendlich M, Klebe G. Utilising Structural Knowledge in Drug Design Strategies: Applications Using Relibase. *J. Mol. Biol* 2003;326:621–636. [PubMed: 12559927]
- (35). Bergner A, Günther J, Hendlich M, Klebe G, Verdonk M. Use of Relibase for retrieving complex 3D interaction patterns including crystallographic packing effects. *Biopolymers (Nucleic Acid Sci.)* 2002;61:99–110.
- (36). Guex, N.; Diemand, A.; Peitsch, MC.; Schwede, T. Swiss-PDB Viewer. <http://www.expasy.org/spdbv/>
- (37). DeLano, WL. The PyMOL Molecular Graphics System (2002) DeLano Scientific. San Carlos, CA, USA: <http://www.pymol.org>
- (38). Wold, S.; Eriksson, L. In *Chemometric Methods in Molecular Design*. In: van de Waterbeemd, H., editor. *Methods and Principles in Medicinal Chemistry*. 2. VCH Publishers, Inc.; New York, NY: 1995. p. 309-317.

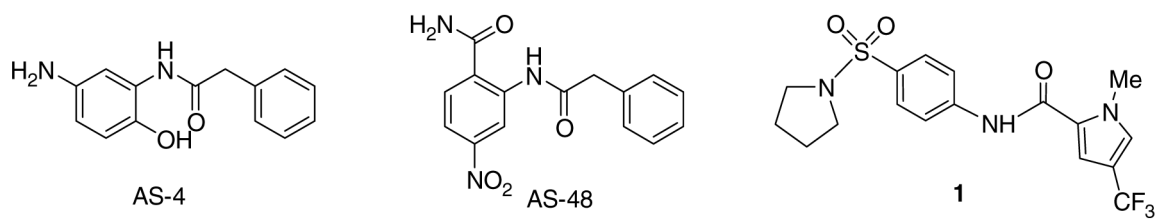


Figure 1.
Structures of compounds AS-4, AS-48 and **1**

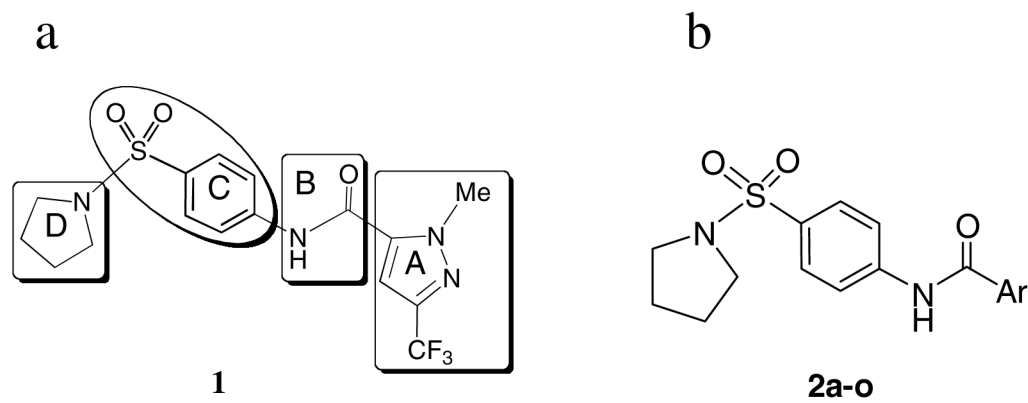


Figure 2. (a) Sectors of compound **1** utilized as an SAR template; (b) Aromatic ring analogs of the compound **1** pyrazole ring, **2a-o**.

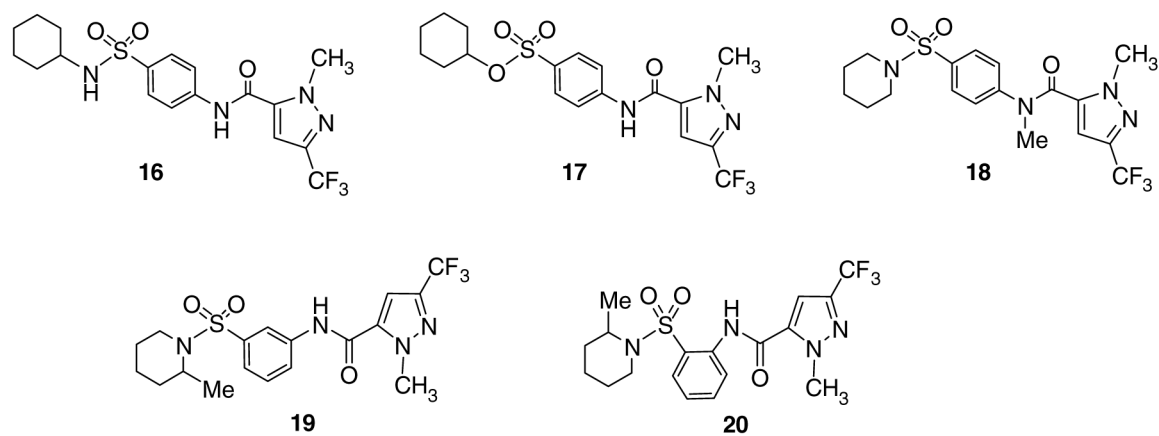


Figure 3.
Variation scaffolds of piperidine analogs.

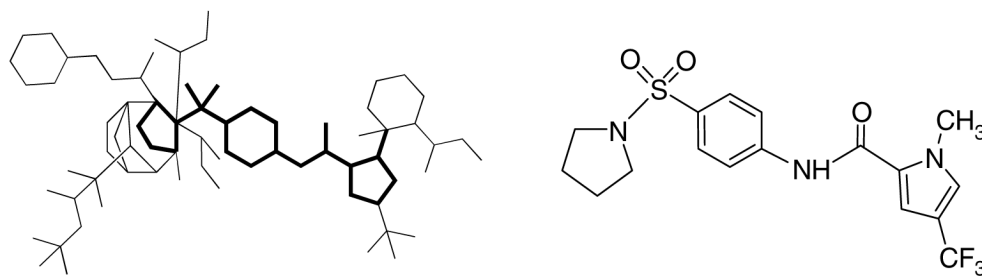


Figure 4. MFTA molecular supergraph (left) formed by the 26 compounds of the training set. The superposition of compound **1** (right) is highlighted to exemplify the alignment

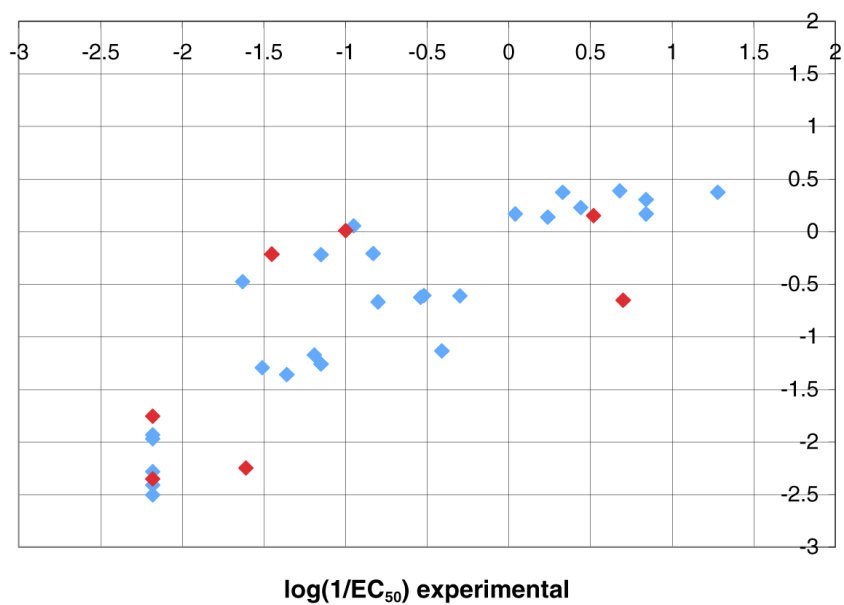


Figure 5. MFTA correlation for the 26 compounds of the training set (blue) and the 7 compounds of the test set (red) based on charge (Q), effective vdW radius (R_e) and lipophilicity (L_q) descriptors.

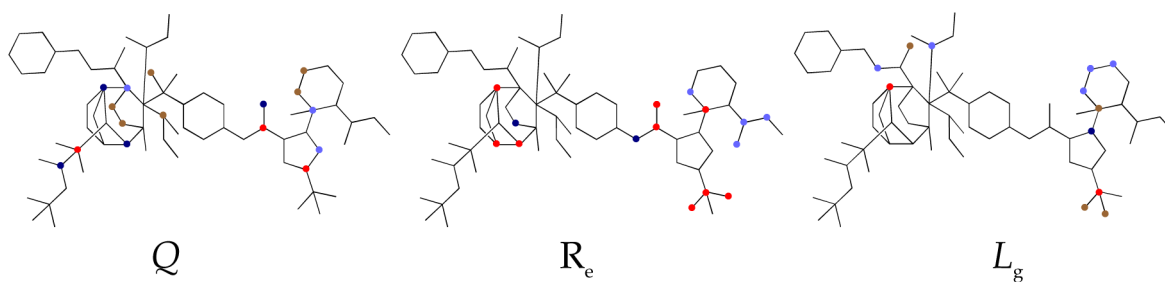


Figure 6. Descriptor impact on activity shown on the molecular supergraph. The QSAR model predicts that increasing the descriptor property at the red and blue positions results in an increase and decrease in activity, respectively.

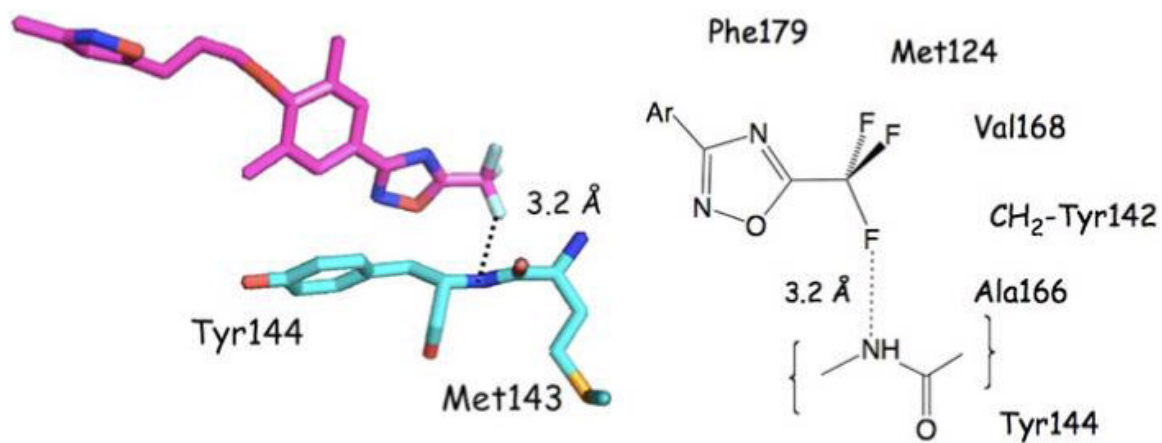


Figure 7. The 1,2,4-oxadiazole terminus of the rhinovirus blocker pleconaril sited in a hydrophobic pocket as determined by X-ray crystallography (INCR). One of the CF₃ fluorine atoms engages in a slightly elongated hydrogen bond with the backbone NH of Tyr144.

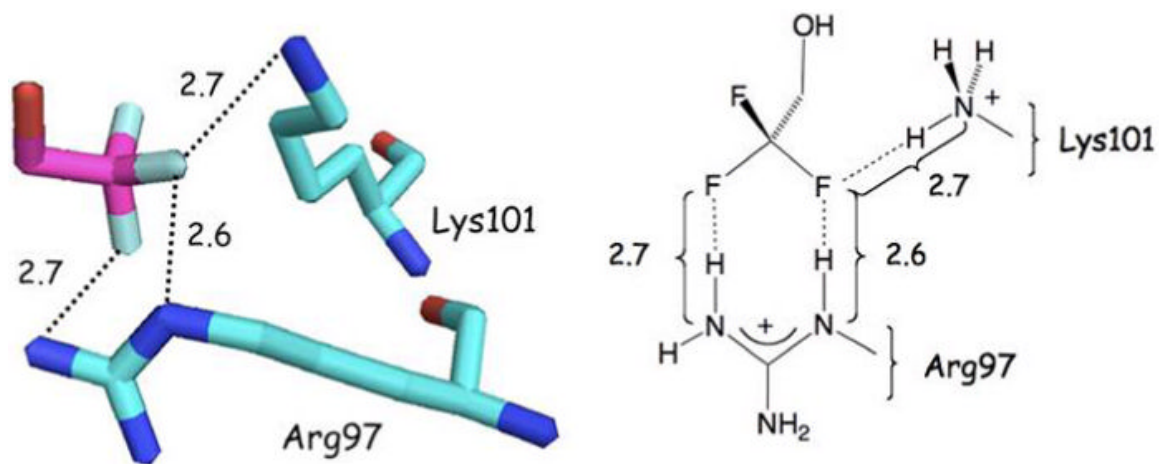


Figure 8. H-Ras 166 in 50% 2,2,2 trifluoroethanol (1P2S) sequesters the CF₃ group of a solvent molecule between Arg97 and Lys101 side chains by bidentate and monodentate hydrogen bonds, respectively. Distances are between F---N atoms. Units for numerical values are Å.

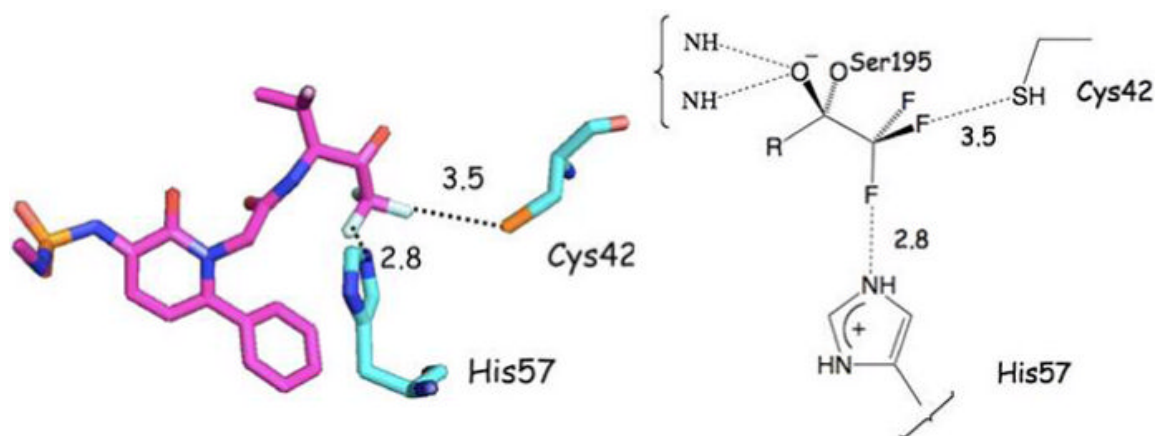


Figure 9.

A trifluoromethyl ketone inhibitor of human leukocyte elastase (1EAS) illustrating an F---HS hydrogen bond and a charge dipole interaction between a ligand C-F bond and His57. Units for numerical values are Å.

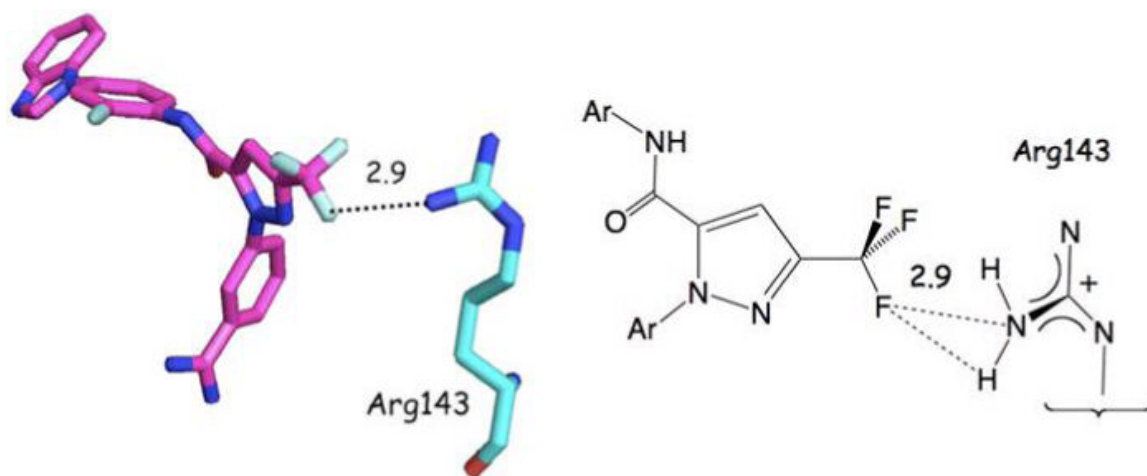
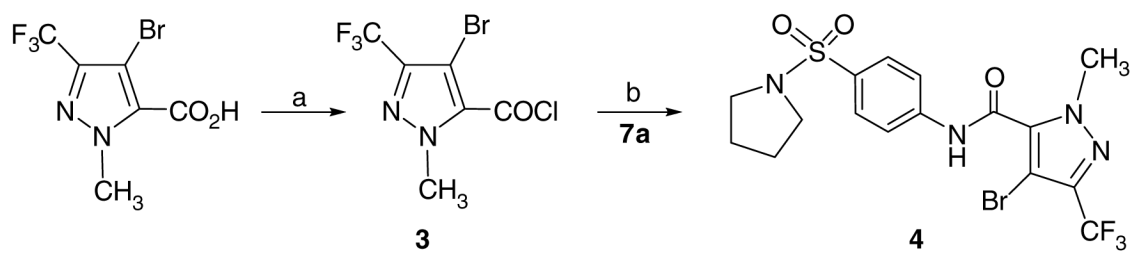
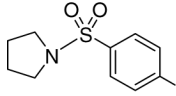


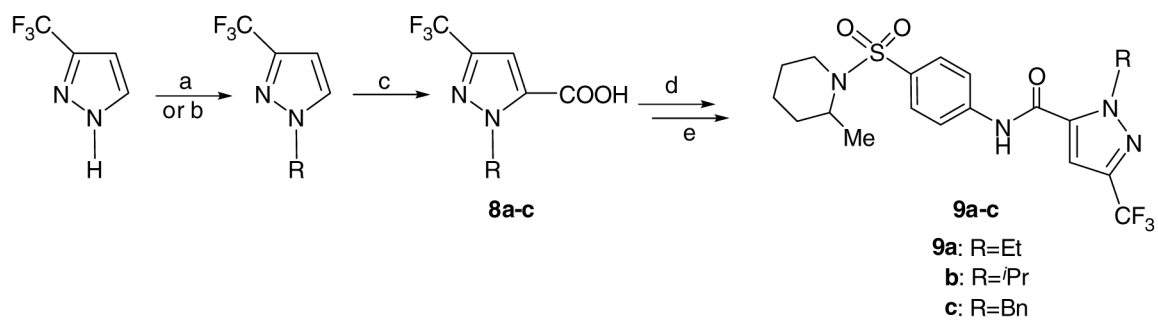
Figure 10. Porcine Factor IXa Complexed to 1-{3-[amino(imino)methyl]phenyl}-N-[4-(1H-benzimidazol-1-yl)-2-fluorophenyl]-3-(trifluoromethyl)-1H-pyrazole-5-carboxamide (1X7A). The CF₃ of the pyrazole ligand interacts tightly with the cationic terminus of the Arg143 side chain. Units for numerical values are Å.



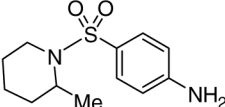
^a Reagents: (a) (COCl)₂, DMF(cat.), CH₂Cl₂, 0°C-rt; (b)  (**7a**), py, CH₂Cl₂, rt.

Scheme 1.

Synthesis of 1-methyl-3-(trifluoromethyl)-4-bromo-N-[4-(pyrrolidinylsulfonyl)phenyl]-1H-pyrazole-5-carboxamide (**4**)^a

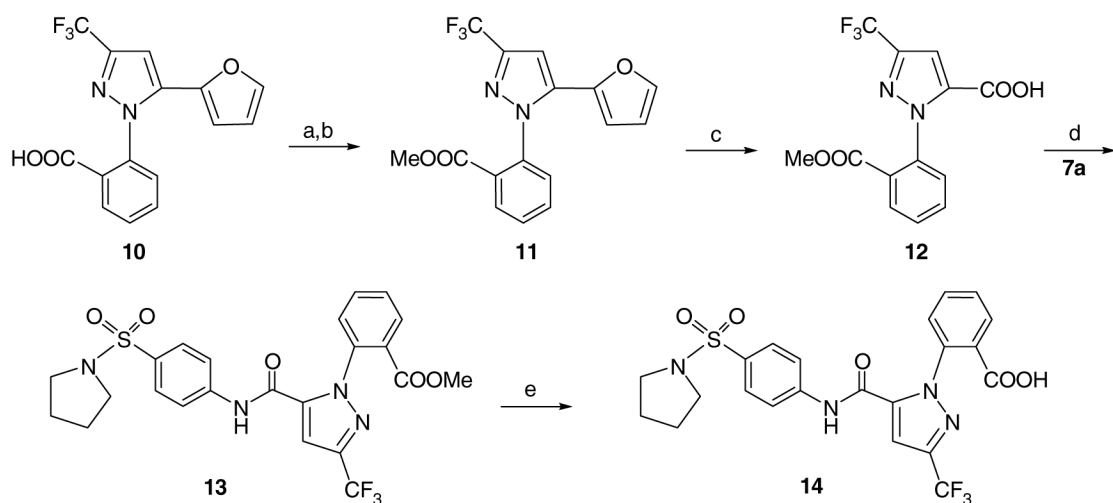


^a Reagents: (a) NaH, benzyl bromide, DMF; or (b) K₂CO₃, RI, DMF ;(c) *n*-BuLi/*i*-Pr₂NH, then CO₂;

(d) (COCl)₂, DMF(cat.), CH₂Cl₂, 0°C-rt; (e)  (**7c**), py, CH₂Cl₂, rt.

Scheme 2.

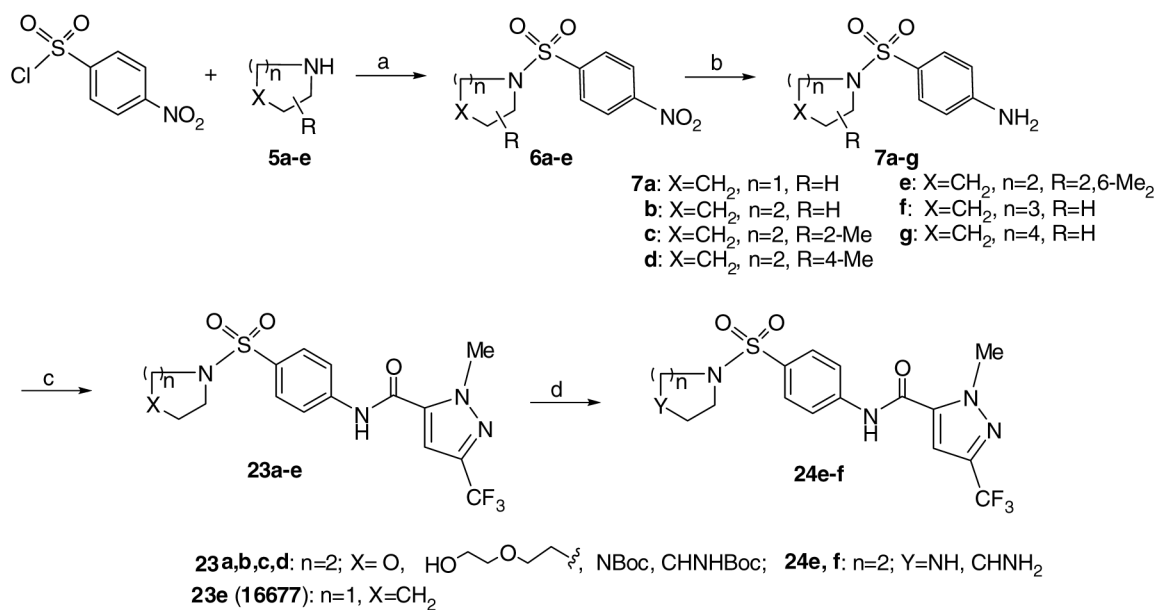
Synthesis of 1-alkyl-3-(trifluoromethyl)-5-carboxamide **9**.^a



^a Reagents: (a) oxalyl chloride; (b) MeOH; (c) KMnO₄, H₂O, acetone; (d) (COCl)₂, DMF(cat.), CH₂Cl₂, 0°C-rt, then py, **7a**, CH₂Cl₂, rt; (e) 50% NaOH, MeOH/H₂O (5:1), room temperature, 5h, then 1N HCl.

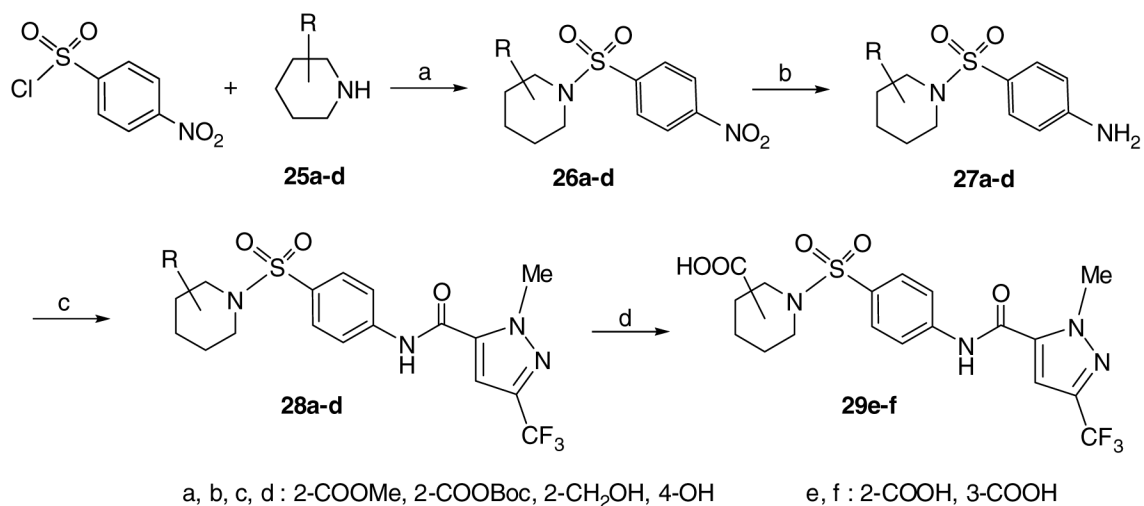
Scheme 3.

Synthesis of 1-[2-carboxy-phenyl]-3-trifluoromethyl-pyrazole analogs



^a Reagents: (a) Py/CH₂Cl₂; (b) Pd/C (10%), H₂ (50psi), 1hr; (c) Py, CH₂Cl₂, 1-methyl-3-trifluoropyrazole-5-acetyl chloride, 2hr; (d) TFA/CH₂Cl₂(3:1), 4hr.

Scheme 4.
Synthesis of derivatives **23** and **24**.



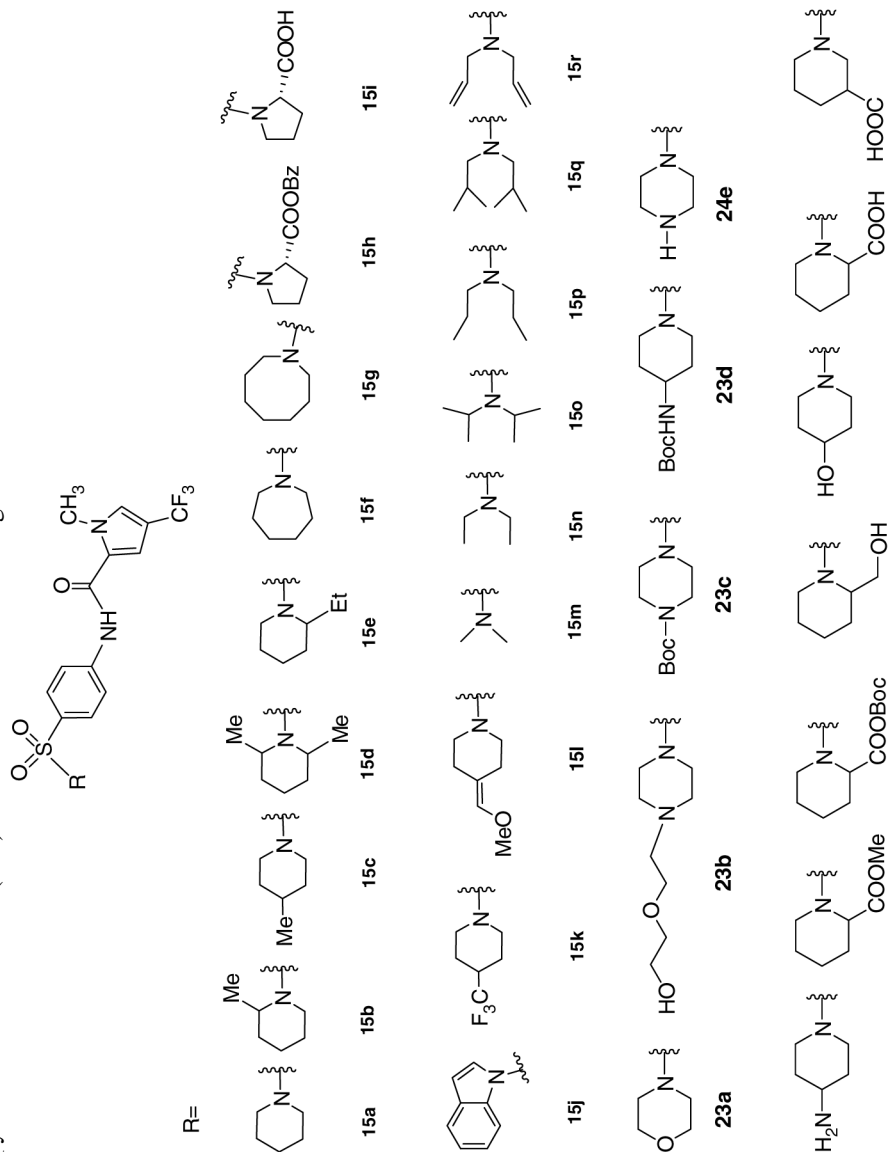
^a Reagents: (a) Py/CH₂Cl₂; (b) Pd/C (10%), H₂ (50psi), 1hr; (c) Py, CH₂Cl₂, 2hr; (d) 50% NaOH, MeOH/H₂O (5:1), room temperature, 5h, then 1N HCl.

Scheme 5.

Synthesis of substituted piperidine derivatives **28** and **29**.

Table 1

Antiviral MV EC₅₀'s, cytotoxicities and selectivity indices for 1-methyl-N-(4-(piperidin-1-ylsulfonyl)phenyl)-3-(trifluoromethyl)-1H-pyrazole-5-carboxamide (**15a**) and other sulfonamide analogs



Entry	EC ₅₀ (μM) (MV-Alaska)			CC ₅₀ (μM) (Vero cells)		SI (CC ₅₀ /EC ₅₀)	
	CPE inhibition ^d	virus titer reduction ^c	MTT cytotoxicity ^d	Trypan blue exclusion assay ^e	CPE + MTT	Titer + Trypan	
4	>75	ND	95 ± 20	ND	<1.3	ND	ND
9a	<2.3	0.055±0.013	30±2.4	ND	ND	ND	ND
9b	>75	ND	>300	ND	ND	ND	ND
9c	>19 ^c	>19 ^b	ND	19 ± 1	ND	ND	ND

Entry	EC ₅₀ (μM) (MV-A1aska)	CC ₅₀ (μM) (Vero cells)	SI (CC ₅₀ /EC ₅₀)			
ID #	CPE inhibition ^d	virus titer reduction ^c	MTT cytotoxicity ^d	Trypan blue exclusion assay ^e	CPE + MTT	Titer + Trypan
13	>75	>75	ND	> 300	ND	ND
14	>75	>75	ND	> 300	ND	ND
15a ^f	<2.3	0.014 ± 0.02	> 300	199 ± 27	> 130	14,214
15b	<2.3	0.029 ± 0.031	> 300	54 ± 3	> 130	1,862
15c	<2.3	0.035 ± 0.035	> 300	53 ± 4	> 130	1,514
15d	<2.3	0.014 ± 0.013	> 300	328 ± 28	> 130	23,429
15e	<2.3	0.087 ± 0.116	> 300	14 ± 2	> 130	160.9
15f	<2.3	0.005 ± 0.0003	> 300	425 ± 65	> 130	85,000
15g	<2.3	0.045 ± 0.034	16 ± 0.8	ND	> 7	ND
15h ^g	14 ± 2	ND	100	ND	7.1	ND
15i ^f	23 ± 10	ND	> 300	ND	> 13	ND
15j ^f	>13 ^b	ND	13 ± 0.7	ND	ND	ND
15k	2.3 ± 0.7	0.02 ± 0.02	159 ± 12	ND	69.1	ND
15l	> 75	ND	92 ± 9.3	ND	< 1.2	ND
15m	6.3 ± 0.6	ND	> 300	ND	> 47.6	ND
15n	<2.3	0.019 ± 0.019	> 300	280 ± 90	> 130	14,737
15o	3.5 ± 0.4	0.53 ± 0.02	> 300	ND	> 85.7	ND
15p	<2.3	0.19 ± 0.32	> 300	ND	> 130	ND
15q	>13.8 ^b	ND	13.8 ± 0.7	ND	ND	ND
15r	3.3 ± 1.4	ND	34 ± 0.9	ND	10.3	ND
16	> 15 ^b	ND	15 ± 0.6	ND	ND	ND
17	> 75	ND	> 300	ND	ND	ND
18	> 75	ND	> 300	ND	ND	ND
19	> 75	ND	286 ± 17	ND	< 3.8	ND
20	> 75	ND	84 ± 23	ND	< 1.1	ND
23a ^f	43 ± 24	ND	> 300	ND	ND	ND
23b	>75	ND	> 300	ND	> 7	ND
23c	> 75	ND	> 300	ND	ND	ND
23d	14.1 ± 6.6	ND	> 300	ND	ND	ND
24e	28 ± 9	ND	126 ± 7	ND	> 21.3	ND
24f ^f	> 75	ND	> 300	ND	4.5	ND
28a	10 ± 5.6	ND	136 ± 3	ND	ND	ND
28b	> 38 ^b	ND	38 ± 1	ND	13.6	ND
28c	<2.3	0.85 ± 0.05	159 ± 40	ND	> 69	ND
28d	6.8 ± 0.9	0.57 ± 0.04	274 ± 19	ND	40.2	ND
29e	> 75	ND	> 300	ND	ND	ND
29f	> 75	ND	> 300	ND	ND	ND

^aEC₅₀ not determined (ND) when CC₅₀ ≤ 15 μM. Values represent averages of four experiments ± SD; highest concentration assessed 75 μM, lowest concentration assessed 2.3 μM.

^bNo virus inhibition detected at CC₅₀ concentration.

^cDetermined only when CPE inhibition-based EC₅₀ concentration < 2.3 μM. Values represent averages of two to four experiments ± SEM; highest concentration assessed 1 μM. (ND: not determined)

^dValues represent averages of at least three experiments ± SD; highest concentration assessed 300 μM.

^eDetermined only when virus titer reduction was assessed and MTT-assay based cytotoxicity > 300 μM. (ND: not determined)

NIH-PA Author Manuscript

NIH-PA Author Manuscript

NIH-PA Author Manuscript

f Published results 15